Phase Coherence of Pairs of Cooper Pairs as Quasi-Long-Range Order of Half-Vortex Pairs in a Two-Dimensional Bilayer System

Feng-Feng Song[1] and Guang-Ming Zhang[1,2,*]
[1]State Key Laboratory of Low-Dimensional Quantum Physics and Department of Physics, Tsinghua University, Beijing 100084, China
[2]Frontier Science Center for Quantum Information, Beijing 100084, China

(Received 18 July 2021; accepted 7 April 2022; published 12 May 2022)

It is known that the loss of phase coherence of Cooper pairs in two-dimensional superconductivity corresponds to the unbinding of vortex-antivortex pairs with the quasi-long-range order in the order-parameter phase field, described by the Berezinskii-Kosterlizt-Thouless (BKT) transition of a 2D XY model. Here we show that the second-order Josephson coupling can induce an exotic superconducting phase in a bilayer system. By using tensor-network methods, the partition function of the 2D classical model is expressed as a product of 1D quantum transfer operator, whose eigenequation can be solved by an algorithm of matrix product states rigorously. From the singularity shown by the entanglement entropy of the 1D quantum analog, various phase transitions can be accurately determined. Below the BKT phase transition, an interlayer Ising long-range order is established at T_{Ising}, and the phase coherence of both intralayers and interlayers is locked together. For two identical layers, the Ising transition coincides with the BKT transition at a multicritical point. For two inequivalent layers, however, there emerges an intermediate quasi-long-range order phase ($T_{\mathrm{Ising}} < T < T_{\mathrm{BKT}}$), where the vortex-antivortex bindings occur in the layer with the larger intralayer coupling, but only half-vortex pairs with topological strings exist in the other layer, corresponding to the phase coherence of pairs of Cooper pairs. So our study provides a promising way to realize the charge-4e superconductivity in a bilayer system.

DOI: 10.1103/PhysRevLett.128.195301

Introduction.—Superconductivity arises from electron pairing and its phase coherence. In conventional Bardeen-Cooper-Schrieffer superconductors, the electron pairing and condensation of Cooper pairs always happen simultaneously, and the superconducting transition is determined by the pairing temperature. In two dimensions, however, the true transition can be substantially below the pairing temperature and is controlled primarily by thermal fluctuations in the phase field of the order parameter [1–7]. In the Ginzburg-Landau theory, when the magnitude fluctuation of the order parameter is frozen, the phase field fluctuation can be characterized by the 2D XY spin model, and the loss of phase coherence among the Cooper pairs corresponds to the unbinding of vortex-antivortex pairs with the quasi-long-range order (quasi-LRO), characterized by the Berezinskii-Kosterlizt-Thouless (BKT) phase transition [8–10].

In recent years there has been increasing interest in a bilayer structure of coupled 2D superconducting systems [11–15]. When a direct Josephson coupling is present, the relative phase of the order parameters is pinned to a fixed value, so both phase locking and phase coherence of the Cooper pairs are characterized by a single BKT transition [16]. However, when the direct Josephson coupling is suppressed [4,5], the second-order Josephson coupling is dominant, and an Ising-like transition for the phase locking occurs at T_{Ising}, which is usually lower than the BKT transition temperature T_{BKT}. For the inequivalent coupled layers, it was argued that there exsits an intermediate phase ($T_{\mathrm{Ising}} < T < T_{\mathrm{BKT}}$) with partial order: one layer is in disordered phase and the other layer has vortex-antivortex pairs with quasi-LRO [17]. Because of the lack of sharp thermodynamic signatures for the BKT transition, it cannot unambiguously determine whether the transition for the identical coupled layers is a single or double transition with an intervening unlocked phase [17]. Actually, the nature of the intermediate phase with partial order has not been fully explored, so it is a great challenge to determine the global phase diagram and calculate the properties of the intermediate phase accurately.

Recently, tensor-network methods have become a powerful tool to characterize correlated quantum many-body phases and their phase transitions in the thermodynamic limit [18,19]. Since the partition function of a 2D statistical model can be represented as a tensor product of a 1D quantum transfer operator [20], the correspondence eigenequation can be efficiently solved by the algorithm of variational uniform matrix product states [21–24]. In this Letter, we apply this method to the bilayer system. According to the singularity displayed by the entanglement

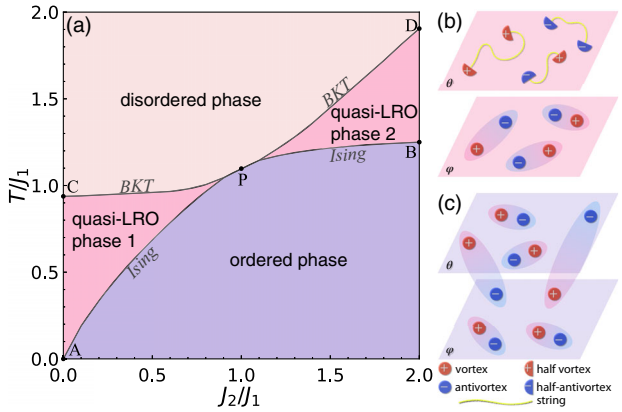

FIG. 1. (a) The finite-temperature phase diagram of the bilayer system. Here we choose $K = 0.5J_1$. In the low-temperature phase, there emerges an interlayer Ising-like long-range order. The BKT and Ising transitions merge together at the point P. (b) The schematic picture of the quasi-LRO phase 2, while the quasi-LRO phase 1 is obtained by switching the upper and lower layers. (c) The schematic picture of the low-temperature ordered phase.

entropy of the 1D quantum analog, various phase transitions can be precisely determined [25,26], and various correlation functions of local observables are calculated rigorously.

The derived global phase diagram is displayed in Fig. 1(a). As the temperature decreases, the BKT transition first occurs before a local interlayer Ising long-range order is established. The Ising transition accompanies the vortex-antivortex bindings in both intralayers and interlayers, as shown in Fig. 1(c). For two identical layers, the Ising transition coincides with the BKT transition at the multicritical point P. However, for two inequivalent layers, we find that the intermediate phase has a quasi-LRO: vortex-antivortex bindings occur only in the layer with the larger intralayer coupling while half-vortex pairs emerge in the other layer, schematically shown in Fig. 1(b). Since the half-vortices are point singularities around which spin directions rotate through an angle π on circumnavigation, each pair of half-vortices is connected by a topological string [27–30]. More importantly, as the quasi-LRO of the phase fields can be viewed as the condensation of the Cooper pairs of 2D superconductivity, the half-vortex pairs with a quasi-LRO imply the condensate of pairs of the Cooper pairs in the absence of phase coherence among the Cooper pairs, corresponding to the charge-4e superconductivity [31–35].

Model and tensor-network methods.—The Hamiltonian of a two-coupled XY spin model on a square lattice is defined by

$$H = -J_1\sum_{\langle i,j\rangle}\cos(\theta_i-\theta_j) - J_2\sum_{\langle i,j\rangle}\cos(\varphi_i-\varphi_j) + K\sum_i\cos(2\theta_i-2\varphi_i), \quad (1)$$

where θ_i and $\varphi_i \in [0, 2\pi]$ are two U(1) phase fields describing the pairing order parameters on the upper and lower layers, respectively, J_1 and J_2 are their respective nearest-neighbor intralayer couplings, and K denotes the second-order Josephson interlayer coupling. Because of the nature of the low-temperature phase, the interlayer coupling is always relevant for *any* finite value of K, and the phase fields θ and φ are no longer two independent U(1) variables. At low temperatures, the relative phase $\sigma_i \equiv \theta_i - \varphi_i$ is reduced to a $\mathbb{Z}_2$ variable, which can be explicitly displayed in the limit of $K \to \infty$, $\varphi_i = \theta_i + \pi s_i/2$, with $s_i = \pm 1$. The reduced Ising-XY coupled model was intensively studied by various numerical methods [36–40].

In the tensor-network framework, the partition function is expressed as a contraction of local tensors defined on the original square lattice, given by

$$Z = \prod_i\iint\frac{d\theta_i d\varphi_i}{(2\pi)^2}\prod_{\langle i,j\rangle}e^{\beta J_1\cos(\theta_i-\theta_j)} \times e^{\beta J_2\cos(\varphi_i-\varphi_j)}e^{-\beta K\cos(2\theta_i-2\varphi_i)}, \quad (2)$$

where $\beta = 1/T$ is the inverse temperature. To obtain its tensor-network representation, we apply a duality transformation that maps the phase variables on each lattice site to the number indices on the nearest-neighbor links. Such a map is achieved by the character decomposition $e^{x\cos\theta} = \sum_{n=-\infty}^{\infty} I_n(x)e^{in\theta}$ for each Boltzmann factor, where $I_n(x)$ is the modified Bessel function of the first kind. Then the partition function is represented as

$$Z = \prod_i\iint\frac{d\theta_i d\varphi_i}{(2\pi)^2}\prod_{l\in\mathcal{L}}\sum_{n_l,m_l,k_l} I_{n_l}(\beta J_1)I_{m_l}(\beta J_2) \times I_{k_l}(-\beta K)e^{in_l(\theta_i-\theta_j)}e^{im_l(\varphi_i-\varphi_j)}e^{i2k_l(\theta_i-\varphi_i)}, \quad (3)$$

where n_l (m_l) runs over every link on the upper (lower) layer, and k_l corresponds to every vertical link between θ_i and φ_i. By integrating out all the phase degrees of freedom, the partition function is transformed into a double tensor network as shown in Fig. 2(a),

$$Z = tTr\prod_i O^{n_3m_3,n_4m_4}_{n_1m_1,n_2m_2}(i), \quad (4)$$

where "tTr" denotes the tensor contraction over all auxiliary links. The details are given in Supplemental Material [41]. As displayed in Fig. 2(b), each local tensor O is defined by

$$O^{n_3m_3,n_4m_4}_{n_1m_1,n_2m_2} = \sum_k\left(\prod_{l=1}^4 I_{n_l}(\beta J_1)I_{m_l}(\beta J_2)\right)^{1/2} \times I_k(\beta K)\delta^{n_3+n_4}_{n_1+n_2+2k}\delta^{m_3+m_4+2k}_{m_1+m_2}, \quad (5)$$

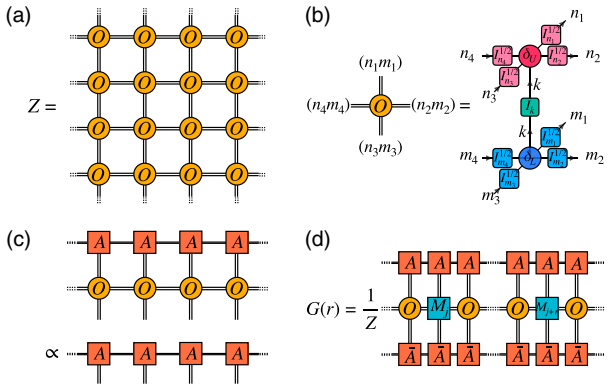

FIG. 2. (a) Tensor-network representation of the partition function. (b) The construction of the local tensor O in the partition function. (c) Eigenequation for the fixed-point UMPS $|\Psi(A)\rangle$ of the 1D quantum transfer operator T. (d) Two-point correlation function represented by contracting a sequence of channel operators.

where the interlayer k indices are summed over and the corresponding intralayer m_l and n_l indices are grouped together. The global $U(1)$ invariance of the bilayer model is encoded in each local tensor: $O^{n_3 m_3, n_4 m_4}_{n_1 m_1, n_2 m_2} \neq 0$ only if $n_1 + m_1 + n_2 + m_2 = n_3 + m_3 + n_4 + m_4$. Since the expansion coefficients in the Bessel function $I_n(x)$ decrease exponentially as increasing n, an accurate truncation can be performed on the virtual indices of the local tensors.

In the tensor-network approach, the row-to-row transfer matrix composed of an infinite row of O tensors is a 1D quantum transfer operator, whose logarithmic form gives rise to a 1D quantum model with complex spin-spin interactions. Under such a correspondence, the finite-temperature properties of the 2D statistical problem are exactly mapped into a 1D quantum model at zero temperature. In the thermodynamic limit, the value of the partition function is determined by the dominant eigenvalues of the transfer operator, whose eigenequation sketched in Fig. 2(c) is

$$T|\Psi(A)\rangle = \Lambda_{\max}|\Psi(A)\rangle, \tag{6}$$

where $|\Psi(A)\rangle$ is the leading eigenvector represented by uniform matrix product states (UMPS) consisting of local A tensors [42]. This eigenequation can be accurately solved by the algorithm of variational uniform matrix product states [21–24], and the largest eigenvector $|\Psi(A)\rangle$ corresponds to the fixed-point solution. The precision of this approximation is controlled by the auxiliary bond dimension D of the local A tensors.

From the fixed-point UMPS for the 1D quantum transfer operator, various physical quantities can be estimated accurately. As far as the phase transitions are concerned, the quantum entanglement entropy is the most efficient measure [43,44], which can be directly determined via the Schmidt decomposition of $|\Psi(A)\rangle$: $S_E = -\sum_{\alpha=1}^{D} s_\alpha^2 \ln s_\alpha^2$, where s_α are the singular values. And the two-point correlation function of the local observable h_i defined by $G(r) = \langle h_j h_{j+r}\rangle$ can be evaluated by the trace of an infinite sequence of channel operators containing two local impurity tensors M_j and M_{j+r}, as shown in Fig. 2(d). The details can be found in Supplemental Material [41].

Phase diagram.—Since the interlayer coupling is always relevant, the structure of the complete phase diagram is *independent* of its value, so we simply choose a practical value $K/J_1 = 0.5$. Importantly, we have noticed that the entanglement entropy S_E of the fixed-point UMPS for the 1D quantum transfer operator exhibits singularity, which provides an accurate criterion to determine the transition points. To obtain the phase diagram, we have to numerically calculate the entanglement entropy under a wide range of intralayer coupling ratios J_2/J_1. In Fig. 3(a), the entanglement entropy along $J_2/J_1 = 1.5$ develops two sharp peaks at $T_{c1} \simeq 1.21J_1$ and $T_{c2} \simeq 1.44J_1$, respectively. When J_2 approaches J_1, these two peaks merge together, leading to a single peak at $T_* \simeq 1.095J_1$, as shown in Fig. 3(b). These peak positions are nearly unchanged under the bond dimensions $D = 90$, 100, 110. So the phase boundaries can be determined with high precision and the complete phase diagram is displayed in Fig. 1(a).

In order to gain insight into the essential physics of different phases, we calculate the specific heat. Within the tensor-network framework, the internal energy per site is calculated as

$$u = -2J_1\langle e^{i(\theta_j - \theta_{j+1})}\rangle - 2J_2\langle e^{i(\varphi_j - \varphi_{j+1})}\rangle + K\langle e^{i(2\theta_j - 2\varphi_j)}\rangle,$$

and the specific heat is obtained by $C_V = \partial u/\partial T$. As shown in Fig. 3(c), along the line $J_2/J_1 = 1.5$, the specific heat exhibits a logarithmic divergence at T_{c1} but a small bump around T_{c2}. However, for $J_2/J_1 = 1$, a single logarithmic singularity is observed at T_* as displayed in

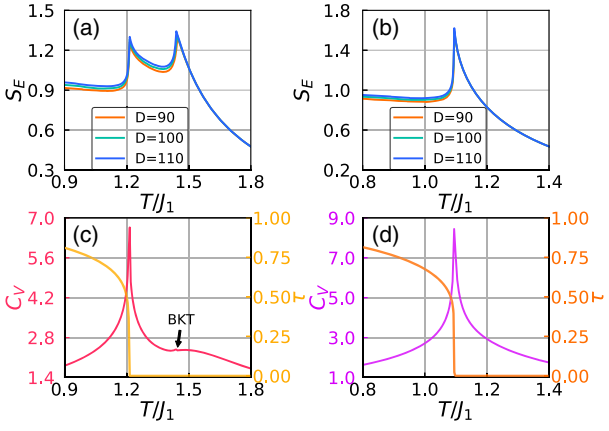

FIG. 3. (a),(b) The entanglement entropy as a function of temperature for $J_2/J_1 = 1.5$ and $J_1 = J_2$, with $K = 0.5J_1$. (c), (d) The specific heat and the local Ising order parameter along $J_2/J_1 = 1.5$ and $J_1 = J_2$, respectively.

TABLE I. Properties of correlation functions in the different phases of the phase diagram in Fig. 1.

	Disordered	Quasi-LRO-1	Quasi-LRO-2	Ordered
$\langle e^{i(\varphi_i-\varphi_j)}\rangle$	$\sim e^{-r/\xi_\varphi}$	$\sim e^{-r/\xi_\varphi}$	$\sim r^{-\eta_\varphi}$	$\sim r^{-\eta_\varphi}$
$\langle e^{i2(\varphi_i-\varphi_j)}\rangle$	$\sim e^{-r/\xi_{2\varphi}}$	$\sim r^{-\eta_{2\varphi}}$	$\sim r^{-\eta_{2\varphi}}$	$\sim r^{-\eta_{2\varphi}}$
$\langle e^{i(\theta_i-\theta_j)}\rangle$	$\sim e^{-r/\xi_\theta}$	$\sim r^{-\eta_\theta}$	$\sim e^{-r/\xi_\theta}$	$\sim r^{-\eta_\theta}$
$\langle e^{i2(\theta_i-\theta_j)}\rangle$	$\sim e^{-r/\xi_{2\theta}}$	$\sim r^{-\eta_{2\theta}}$	$\sim r^{-\eta_{2\theta}}$	$\sim r^{-\eta_{2\theta}}$
$\langle e^{i(\theta_i-\varphi_j)}\rangle$	$\sim e^{-r/\xi_{\theta\varphi}}$	$\sim e^{-r/\xi_{\theta\varphi}}$	$\sim e^{-r/\xi_{\theta\varphi}}$	$\sim r^{-\eta_{\theta\varphi}}$
$\langle e^{i(\sigma_i-\sigma_j)}\rangle$	$\sim e^{-r/\xi_\sigma}$	$\sim e^{-r/\xi_\sigma}$	$\sim e^{-r/\xi_\sigma}$	$\sim$const

Fig. 3(d). The logarithmic specific heat at the lower temperature reminds us of a 2D Ising phase transition with a $\mathbb{Z}_2$ symmetry breaking, while the small bump at the higher temperature indicates the nearby BKT transition.

At low temperatures, since the relative phase field $\sigma_i \equiv \theta_i - \varphi_i$ is reduced to a $\mathbb{Z}_2$ variable, a local interlayer Ising order parameter can be defined by $\tau = \langle \sin \sigma_i \rangle$. As shown in Figs. 3(c) and 3(d), τ is finite below T_{c1}, indicating that the phase lock occurs between the upper and lower layers. When $J_2/J_1 = 1$, the Ising transition coincides with the BKT transition exactly at the multicritical point P, where there is an interplay between the Ising and BKT degrees of freedom at the microscopic level, exhibiting a new universality class of critical properties with emerged supersymmetry [45].

Correlation functions and spin stiffness.—To further explore the nature of the intermediate temperature phase, we calculate the two-point correlation functions of the XY spins and nematic spins, which represent the integer vortices and half-integer vortices variables in the bilayer system, respectively. The results are summarized in Table I.

For $J_2/J_1 > 1$, the spin-spin correlation function of the lower layer $G_\varphi(r)$ starts to decay algebraically at T_{c2} as the temperature decreases. When approaching T_{c2} from above, the spin correlation length ξ_φ is well fitted by an exponentially divergent form,

$$\xi(T) \propto \exp\left(\frac{b}{\sqrt{T - T_C}}\right), \qquad T \to T_C^+, \tag{7}$$

where b is a nonuniversal positive constant. This is the characteristic feature of the BKT transition. Below T_{c1}, the spin-spin correlation functions of both the intralayer $G_\theta(r)$ and the interlayer $G_{\theta\varphi}(r)$ exhibit the algebraic behavior, implying the vortex-antivortex bindings in both intralayers and interlayers, a fully phase-coherent state of the Cooper pairs in the bilayer system.

When we focus on the quasi-LRO-2 phase, the spin-spin correlation function $G_\varphi(r)$ in the lower layer decays algebraically, while in the upper layer it is the correlation function of the nematic spins $G_{2\theta}(r)$ that exhibits an algebraic behavior, instead of the correlation function of the XY spins $G_\theta(r)$:

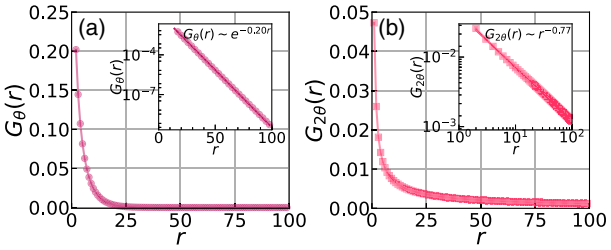

FIG. 4. The properties of the quasi-LRO phase 2 when $J_2/J_1 = 1.5$, $K/J_1 = 0.5$, and $T/J_1 = 1.3$. (a) The correlation function of the XY spins shows an exponential decay. The inset is an exponential fitting. (b) The correlation function of the nematic spins exhibits a power law decay. The inset is fitted by a power law.

$$G_\theta(r) = \langle e^{i(\theta_j - \theta_{j+r})} \rangle \sim e^{-r/\xi_\theta},$$
$$G_{2\theta}(r) = \langle e^{i(2\theta_j - 2\theta_{j+r})} \rangle \sim r^{-\eta_{2\theta}}. \tag{8}$$

For a given value of $J_2/J_1 = 1.5$ and $T/J_1 = 1.3$, the comparison between the spin-spin correlation function and nematic correlation function is displayed in Figs. 4(a) and 4(b). Such a behavior indicates that the integer vortices in the upper layer are fractionalized into half-integer vortex pairs due to the presence of the interlayer squared cosine interaction. Since the half-integer vortices are pointlike topological defects about which the phase angles of spins wind by π, each pair of half-vortices should be connected by a topological string across which spins are antiparallel. Because the integer vortex-antivortex pairs with quasi-LRO are regarded as the phase condensation of the Cooper pairs in 2D, the half-integer vortex pairs with quasi-LRO can be regarded as the condensation of pairs of the Cooper pairs in the absence of the phase coherence among the Cooper pairs [31,32]. Such a phenomenon is just the characteristics of the charge-4e superconductivity [33–35].

To access the superfluid response of the bilayer system, we calculate the spin stiffness or the helicity modulus defined by the second derivative of the free-energy density with respect to a twist v along a given direction [46,47], $\rho_s = (\partial^2 f/\partial^2 v)|_{v=0}$. The twist needs to be taken in a way that respects the joint U(1) symmetry of the coupled bilayer, and the spin stiffness is expressed in terms of two-point functions within the framework of tensor-network methods [48,49]. Since the process is more technical, the details are given in the Supplemental Material [41]. The jump of spin stiffness should be altered from the BKT predictions $\rho_s/T_{\mathrm{BKT}} = 2/\pi$ due to the emergence of half-vortices [50]. In Fig. 5, the numerical spin stiffness as a function of temperature is shown for $J_2/J_1 = 1.0$–1.8 with the interlayer coupling $K/J_1 = 0.5$. It can be seen that the spin stiffness starts to dramatically increase from zero around the BKT transition temperature T_{c2}. When the temperature decreases, a cusp point forms in the further increase of the spin stiffness, corresponding to the Ising phase transition T_{c1} precisely. Surprisingly, the cusp points

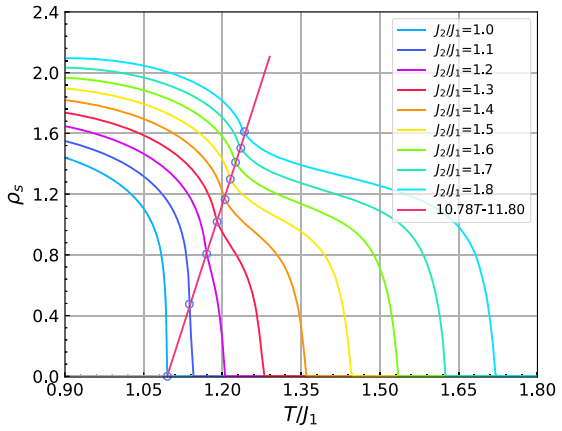

FIG. 5. The spin stiffness as a function of temperature for given values of J_2/J_1. The interlayer coupling is chosen as $K = 0.5J_1$, and the bond dimension of the local tensor is $D = 110$. The red straight line indicates the temperature of the Ising transition.

for given values of J_2/J_1 sit on a straight line, which is a key experimental feature of the presence of the Ising phase transition within the superconducting phase.

Conclusion.—We have used the tensor-network methods to study the bilayer system of two-coupled 2D XY spin models. The global finite-temperature phase diagram has been accurately determined. It has been found that, as the temperature decreases, the BKT transition always happens above the phase locking of the bilayer system, which corresponds to an interlayer Ising long-range order. More importantly, for two inequivalent coupled bilayers, there exists an intervening unlocked phase, where the half-integer vortex pairs form in one layer with the smaller intralayer coupling, coexisting with the integer vortex-antivortex pairs in the other layer. When a weak direct Josephson coupling is also present, we have further proved that the Ising phase transition below the BKT transition survives and the main results of this work are still valid, because two local minima always exist to lock the phase fields of the upper and lower layers.

Recently, a new family of superconductors $ACa_2Fe_4As_4F_2$ (A = K, Rb, Cs) has synthesized [51], and these compounds can be viewed as an intergrowth of AFe_2As_2 and CaFeAsF layers. The transport and magnetic measurements on single crystals of $CsCa_2Fe_4As_4F_2$ showed a large resistivity anisotropy that tends to increase with decreasing temperature, and the 2D superconducting fluctuations have been observed [52]. The evolution of the in-plane penetration depth shows an inflection point around 10 K, indicating that a potentially "magnetic" phase appears but does not compete with superconductivity [53]. These features may be related to the formation of the interlayer Ising long-range order and the manifestation of the phase coherence of pairs of Cooper pairs revealing a cusp point in the spin stiffness. Therefore, these compounds are good candidate systems to explore the charge-4e superconductivity.

The authors are indebted to Qi Zhang for his stimulating discussions. The research is supported by the National Key Research and Development Program of MOST of China (2017YFA0302902).

*gmzhang@tsinghua.edu.cn

[1] M. R. Beasley, J. E. Mooij, and T. P. Orlando, Phys. Rev. Lett. **42**, 1165 (1979).
[2] V. J. Emery and S. A. Kivelson, Nature (London) **374**, 434 (1995).
[3] E. W. Carlson, S. A. Kivelson, V. J. Emery, and E. Manousakis, Phys. Rev. Lett. **83**, 612 (1999).
[4] Q. Li, M. Hücker, G. D. Gu, A. M. Tsvelik, and J. M. Tranquada, Phys. Rev. Lett. **99**, 067001 (2007).
[5] J. F. Ding, X. Q. Xiang, Y. Q. Zhang, H. Liu, and X. G. Li, Phys. Rev. B **77**, 214524 (2008).
[6] B. L. Kang, M. Z. Shi, S. J. Li, H. H. Wang, Q. Zhang, D. Zhao, J. Li, D. W. Song, L. X. Zheng, L. P. Nie *et al.*, Phys. Rev. Lett. **125**, 097003 (2020).
[7] B. D. Faeth, S.-L. Yang, J. K. Kawasaki, J. N. Nelson, P. Mishra, C. T. Parzyck, C. Li, D. G. Schlom, and K. M. Shen, Phys. Rev. X **11**, 021054 (2021).
[8] V. L. Berezinskii, Sov. Phys. JETP **32**, 493 (1971).
[9] J. M. Kosterlitz and D. J. Thouless, J. Phys. C **6**, 1181 (1973).
[10] J. M. Kosterlitz, J. Phys. C **7**, 1046 (1974).
[11] T. A. Bojesen, E. Babaev, and A. Sudbø, Phys. Rev. B **88**, 220511(R) (2013).
[12] T. A. Bojesen, E. Babaev, and A. Sudbø, Phys. Rev. B **89**, 104509 (2014).
[13] M. Kobayashi, M. Eto, and M. Nitta, Phys. Rev. Lett. **123**, 075303 (2019).
[14] G. Bighin, N. Defenu, I. Nándori, L. Salasnich, and A. Trombettoni, Phys. Rev. Lett. **123**, 100601 (2019).
[15] M. Zeng, L.-H. Hu, H.-Y. Hu, Y.-Z. You, and C. Wu, arXiv:2102.06158.
[16] N. Parga and J. Van Himbergen, Solid State Commun. **35**, 607 (1980).
[17] E. Granato and J. M. Kosterlitz, Phys. Rev. B **33**, 4767 (1986).
[18] F. Verstraete, V. Murg, and J. Cirac, Adv. Phys. **57**, 143 (2008).
[19] R. Orús, Ann. Phys. (Amsterdam) **349**, 117 (2014).
[20] J. Haegeman and F. Verstraete, Annu. Rev. Condens. Matter Phys. **8**, 355 (2017).
[21] V. Zauner-Stauber, L. Vanderstraeten, M. T. Fishman, F. Verstraete, and J. Haegeman, Phys. Rev. B **97**, 045145 (2018).
[22] M. T. Fishman, L. Vanderstraeten, V. Zauner-Stauber, J. Haegeman, and F. Verstraete, Phys. Rev. B **98**, 235148 (2018).
[23] L. Vanderstraeten, J. Haegeman, and F. Verstraete, Sci. Post Phys. Lect. Notes, 7 (2019).10.21468/SciPostPhysLectNotes.7
[24] L. Vanderstraeten, B. Vanhecke, A. M. Läuchli, and F. Verstraete, Phys. Rev. E **100**, 062136 (2019).
[25] Z.-Q. Li, L.-P. Yang, Z. Y. Xie, H.-H. Tu, H.-J. Liao, and T. Xiang, Phys. Rev. E **101**, 060105(R) (2020).

[26] F.-F. Song and G.-M. Zhang, Phys. Rev. B **103**, 024518 (2021).
[27] D. H. Lee and G. Grinstein, Phys. Rev. Lett. **55**, 541 (1985).
[28] D. B. Carpenter and J. T. Chalker, J. Phys. Condens. Matter **1**, 4907 (1989).
[29] Y. Shi, A. Lamacraft, and P. Fendley, Phys. Rev. Lett. **107**, 240601 (2011).
[30] P. Serna, J. T. Chalker, and P. Fendley, J. Phys. A **50**, 424003 (2017).
[31] B. Douçot and J. Vidal, Phys. Rev. Lett. **88**, 227005 (2002).
[32] E. Babaev, Nucl. Phys. **B686**, 397 (2004).
[33] E. Berg, E. Fradkin, and S. A. Kivelson, Nat. Phys. **5**, 830 (2009).
[34] Y.-F. Jiang, Z.-X. Li, S. A. Kivelson, and H. Yao, Phys. Rev. B **95**, 241103(R) (2017).
[35] R. M. Fernandes and L. Fu, Phys. Rev. Lett. **127**, 047001 (2021).
[36] M. Y. Choi and S. Doniach, Phys. Rev. B **31**, 4516 (1985).
[37] E. Granato, J. M. Kosterlitz, J. Lee, and M. P. Nightingale, Phys. Rev. Lett. **66**, 1090 (1991).
[38] J. Lee, E. Granato, and J. M. Kosterlitz, Phys. Rev. B **44**, 4819 (1991).
[39] M. S. Li and M. Cieplak, Phys. Rev. B **50**, 955 (1994).
[40] M. P. Nightingale, E. Granato, and J. M. Kosterlitz, Phys. Rev. B **52**, 7402 (1995).
[41] See Supplemental Material at http://link.aps.org/supplemental/10.1103/PhysRevLett.128.195301 for a detailed derivation of the tensor-network representation, the calculations of physical quantities based on the VUMPS algorithm, the fitting of conformal data, and the discussion about the first-order interlayer Josephson coupling.
[42] V. Zauner-Stauber, L. Vanderstraeten, M. T. Fishman, F. Verstraete, and J. Haegeman, Phys. Rev. B **97**, 045145 (2018).
[43] G. Vidal, J. I. Latorre, E. Rico, and A. Kitaev, Phys. Rev. Lett. **90**, 227902 (2003).
[44] F. Pollmann, S. Mukerjee, A. M. Turner, and J. E. Moore, Phys. Rev. Lett. **102**, 255701 (2009).
[45] L. Huijse, B. Bauer, and E. Berg, Phys. Rev. Lett. **114**, 090404 (2015).
[46] M. E. Fisher, M. N. Barber, and D. Jasnow, Phys. Rev. A **8**, 1111 (1973).
[47] D. R. Nelson and J. M. Kosterlitz, Phys. Rev. Lett. **39**, 1201 (1977).
[48] L. Vanderstraeten, M. Mariën, F. Verstraete, and J. Haegeman, Phys. Rev. B **92**, 201111(R) (2015).
[49] L. Vanderstraeten, J. Haegeman, P. Corboz, and F. Verstraete, Phys. Rev. B **94**, 155123 (2016).
[50] D. M. Hübscher and S. Wessel, Phys. Rev. E **87**, 062112 (2013).
[51] Z.-C. Wang, C.-Y. He, S.-Q. Wu, Z.-T. Tang, Y. Liu, A. Ablimit, C.-M. Feng, and G.-H. Cao, J. Am. Chem. Soc. **138**, 7856 (2016).
[52] Z.-C. Wang, Y. Liu, S.-Q. Wu, Y.-T. Shao, Z. Ren, and G.-H. Cao, Phys. Rev. B **99**, 144501 (2019).
[53] F. K. K. Kirschner, D. T. Adroja, Z.-C. Wang, F. Lang, M. Smidman, P. J. Baker, G.-H. Cao, and S. J. Blundell, Phys. Rev. B **97**, 060506(R) (2018).